Research Square

Preprints are preliminary reports that have not undergone peer review.
They should not be considered conclusive, used to inform clinical practice,
or referenced by the media as validated information.

Acoustic control of Rayleigh-regime liquid-jet breakup using a through-hole MHz transducer

Kha Nguyen
University of California San Diego
Kareem Ahmed
University of Central Florida
James Friend
jamesfriend@wustl.edu

Washington University in St. Louis

Research Article

Keywords: liquid jet breakup, Rayleigh–Plateau instability, acoustic forcing, high-speed shadowgraphy, capillary waves, wetting, reduced-order correlation

Posted Date: September 2nd, 2026

DOI: https://doi.org/10.21203/rs.3.rs-10528285/v1

License: This work is licensed under a Creative Commons Attribution 4.0 International License.
Read Full License

Additional Declarations: No competing interests reported.

Acoustic control of Rayleigh-regime liquid-jet breakup using a through-hole MHz transducer

K. Nguyen[1], K. Ahmed[2], J. Friend[1,3*]

[1]Medically Advanced Devices Laboratory, Center for Medical Devices, Department of Mechanical and Aerospace Engineering, University of California San Diego, La Jolla, CA, 92093-0411, USA.

[2]Propulsion and Energy Research Lab, Department of Mechanical and Aerospace Engineering, University of Central Florida, Orlando, FL, 32816, USA.

[3]Medically Advanced Devices Laboratory, Department of Mechanical Engineering and Materials Science, Washington University in St. Louis, 1 Brookings Drive, St. Louis, MO, 63130, USA.

*Corresponding author(s). E-mail(s): jamesfriend@wustl.edu;

Abstract

This experimental study demonstrates MHz-order acoustic control of Rayleigh-regime liquid-jet breakup using a compact through-hole lithium niobate thickness-mode transducer integrated at the nozzle exit and driven near its 6.7 MHz resonance. Jet dynamics were measured by high-speed shadowgraphy at 50 000 fps, and breakup lengths were obtained from instantaneous jet-length records using an autocorrelation-based method that identifies statistically separated breakup events. Acoustic actuation produced visible interfacial corrugations and reduced the normalized breakup length, $\boldsymbol{L_b/d}$, for both water and glycerol–water jets. In water, the response was threshold-like at low Weber number and weakened as the jet velocity increased to We $\simeq$ **50**. A reduced-order threshold correlation, fit to the water amplitude and velocity sweeps, captured this abrupt shortening and the subsequent loss of actuation efficacy. More viscous glycerol–water mixtures shortened immediately at low forcing, indicating a distinct acoustic-coupling regime rather than a universal collapse of the water response. A wetting-control experiment showed that liquid spreading at the nozzle base can also shorten the jet, so the measured response reflects coupled radiation-pressure forcing, capillary-wave feedback, and wetting-mediated disturbance injection. Resolved droplet tracking further showed that MHz excitation changes the visible gate-crossing droplet population, although sub-resolution mist and micron-scale atomization were not measured. These results establish through-hole MHz actuation as a compact route for modifying free-surface jet breakup and provide a repeatable image-analysis protocol for experimental-fluid-mechanics measurements.

Keywords: liquid jet breakup; Rayleigh–Plateau instability; acoustic forcing; high-speed shadowgraphy; capillary waves; wetting; reduced-order correlation

1 Introduction

The breakup of a round liquid jet in quiescent air is governed by the Rayleigh–Plateau instability, in which surface tension causes the jet to fragment into droplets to minimize interfacial area (Rayleigh 1878; Eggers

and Villermaux 2008). This phenomenon underpins a broad range of industrial and scientific applications, including fuel atomization, inkjet printing, pharmaceutical spray generation, and droplet-based microfluidics (Lin 2003; Lefebvre and McDonell 2017). A persistent practical objective across these fields is the controlled reduction of the breakup length, which can yield earlier droplet production, finer sprays, narrower droplet-size distributions, and more efficient atomization (Lefebvre and McDonell 2017). The theoretical framework for predicting the natural breakup of a cylindrical jet was established by Rayleigh and extended to include viscous and aerodynamic effects by Weber and later reviews of jet and spray formation (Rayleigh 1878; Weber 1931; Lin and Reitz 1998; Eggers and Villermaux 2008).

One established route to shortening a jet's breakup length is the controlled introduction of external perturbations. Mechanical excitation via piezoelectric elements driving pressure fluctuations inside a liquid chamber has been studied extensively in the context of continuous inkjet printing and forced capillary jets (Donnelly and Glaberson 1966; Goedde and Yuen 1970; Kalaaji et al. 2003; Lad and Murthy 2016; Yang et al. 2019). Electric field forcing can also destabilize jets (Collins et al. 2007), though this approach is restricted to conducting or dielectric fluids. Magnetic forcing requires magnetically susceptible media (Shimasaki and Taniguchi 2011). Each of these methods imposes constraints on the fluid properties, device geometry, or forcing pathway.

Acoustic radiation pressure offers a comparatively fluid-agnostic route, since it acts on liquid–gas interfaces regardless of the liquid's electrical or magnetic properties. However, many acoustic or vibration-based jet-breakup studies have employed frequencies below the MHz range, where the dominant mechanism is direct mechanical modulation of the nozzle, chamber, or imposed inlet disturbance (Lad and Murthy 2016; Yang et al. 2019). At those frequencies, the acoustic wavelength in the liquid is much larger than the jet diameter, and the jet responds primarily through hydrodynamic forcing. Acoustic radiation pressure does not necessarily promote capillary breakup. It has previously been used to suppress the Rayleigh–Plateau instability of liquid bridges through externally applied radiation stresses (Marr-Lyon et al. 1997, 2001). More directly, Bertin et al. (2010) demonstrated that an ultrasonic field injected axially and guided along a liquid column can generate radial radiation stresses that stabilize the column against capillary disturbances.

The physics qualitatively changes at MHz-order frequencies. Frommhold et al. (2014) used a 1.8 MHz disturbance to create monodisperse droplets, though the acoustic waves were not applied at the nozzle exit. For MHz-order acoustic excitation of sessile droplets, visible capillary waves can arise through a pressure–interface feedback mechanism after a finite onset threshold (Zhang et al. 2023). That observation motivates the question of whether analogous MHz-order forcing can be coupled into a free cylindrical jet at the nozzle exit to control its breakup length.

The nozzle orifice exit is a natural coupling point for this mechanism. The surface disturbance that ultimately produces pinch-off is convected downstream within the fluid jet from the orifice exit, and the

breakup length depends logarithmically on the effective initial disturbance amplitude. An acoustic source placed directly at the exit can therefore modify both the initial capillary disturbance and the local wetting state. In the present system, a lithium niobate thickness-mode transducer is drilled to form the flow passage itself, so the liquid exits through a vibrating piezoelectric element rather than through a passive nozzle followed by a remote forcing region.

In this work, we demonstrate that MHz-order acoustic excitation oriented along the jet propagation direction and applied directly at the nozzle exit produces a pronounced reduction in the Rayleigh-regime breakup length of cylindrical liquid jets in quiescent air. Driven at 6.7 MHz, corresponding to a resonance of the piezoelectric transducer comprising the orifice exit, the excitation frequency is far above the natural Rayleigh-Plateau instability frequency of the fluid jet. Using the notation of Eggers and Villermaux (2008), using such a high frequency produces a reduced wavenumber $x = \frac{\pi d}{\lambda} = 14.2$, where d is the orifice diameter and λ is the axial wavelength of the driving disturbance, far above the range $0 < x < 1$ over which the jet would be driven unstable via the Rayleigh-Plateau instability.[1] We integrate a through-hole thickness-mode lithium niobate transducer into a compact nozzle assembly driven near a 7 MHz resonance and characterize jet dynamics using high-speed shadowgraphy at 50 000 fps. We introduce an autocorrelation-based image-analysis method to isolate statistically separated breakup lengths L_b from instantaneous jet-length time series. We then show how the normalized breakup length depends on the normalized acoustic forcing amplitude $u^* = \dot{\xi}_p / u_0$, the Weber number We, the Ohnesorge number Oh, and the nozzle-base wetting state. We also quantify optically resolved gate-crossing droplet distributions above a conservative pixel-scale cutoff, allowing the breakup-length measurements to be compared with the size distribution of visible detached fragments. Finally, we include a reduced-order correlation for the water data. Its longer derivation is placed in the Supplementary Information.

2 Experimental methods

A compact through-hole lithium niobate thickness-mode transducer was used as the nozzle so that acoustic excitation was applied directly at the jet exit. The device was fabricated from a 500 µm-thick, 127.68° Y-rotated lithium niobate chip with Ti/Au electrodes on both faces. A 1 mm through-hole was drilled through the chip and aligned with a stainless-steel tube inside a three-dimensional printed fixture (Fig. 1). The transducer was driven near its thickness resonance using a signal generator and RF amplifier, while voltage and current were measured at the device to estimate the delivered electrical input. Surface particle velocity $\dot{\xi}_p$ at resonance was measured separately by laser Doppler vibrometry and was used to define the normalized acoustic forcing $u^* = \dot{\xi}_p / u_0$. Full fabrication and characterization details are provided in Supplementary Sec. S1.

[1] The convected form of this reduced wavenumber in Eggers and Villermaux (2008) is likewise very large: $x_{\mathrm{conv}} = \frac{\pi d f}{v_j} \approx 3.3 \times 10^4$ with f as the excitation frequency and v_j the jet velocity. Either way, the direct excitation of the Rayleigh-Plateau instability from such a high frequency is implausible.

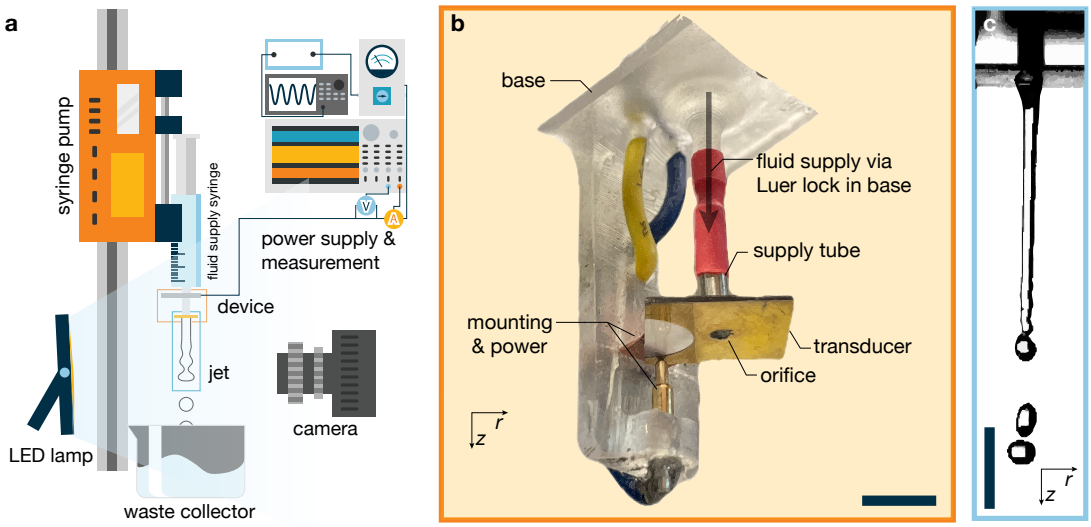


Fig. 1 Experimental arrangement for acoustic control of liquid-jet breakup. (a) Schematic of the syringe-pump, electrical-actuation, and high-speed-imaging setup. For each condition, 46,560 frames were recorded at 50,000 fps. (b) Close-up of the nozzle coupled to the through-hole thickness-mode transducer and compact electrical connection. (c) Representative shadowgraph image of the cylindrical jet. Both scale bars are 5 mm.

Flow was supplied by a syringe pump and independently checked gravimetrically. After each change in flow rate or acoustic forcing, the jet was allowed to reach steady operation for 5 s before recording. The jet was backlit with a diffuse LED source and imaged at 50 000 fps. Experiments were conducted with DI water over $Q = 30\,\text{mL/min}$–$90\,\text{mL/min}$ and with glycerol–water mixtures at $Q = 30\,\text{mL/min}$. All primary parametric sweeps were performed on a single nozzle–transducer assembly to avoid changes in exit geometry. The corresponding flow conditions were expressed as

$$\text{We} = \frac{\rho u_0^2 d}{\sigma}, \qquad \text{Oh} = \frac{\mu}{\sqrt{\rho \sigma d}}, \qquad \text{Re} = \frac{\rho u_0 d}{\mu}, \tag{1}$$

where u_0 is the mean exit velocity, $d = 1\,\text{mm}$ is the nozzle diameter, and ρ, σ, and μ are the liquid density, surface tension, and dynamic viscosity. Fluid properties, flow conditions, and processing thresholds are listed in Supplementary Tables S1 and S2. All data associated with this manuscript is available online at https://doi.org/10.6075/J02N52F5.

Breakup length was obtained from high-speed image sequences as an event-averaged intact length. For each frame, the instantaneous jet length $L_j(t)$ was defined as the distance from the nozzle exit to the first liquid disconnection. Candidate breakup events were identified as local minima of $L_j(t)$, retained only when their prominence exceeded 30% of the video-specific jet-length range and when adjacent retained minima were separated by at least twice the first-zero autocorrelation time of $L_j(t)$. The reported breakup length L_b is the mean of these statistically separated event minima and is reported as L_b/d; error bars denote the standard deviation of the retained event-wise lengths. Comparison between these two approaches is shown in Fig. 2.

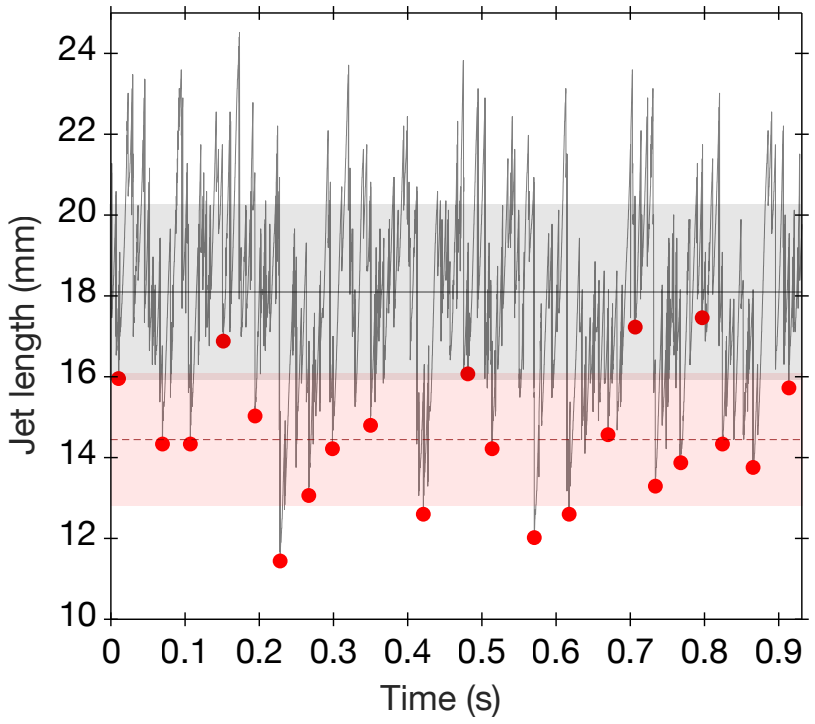


Fig. 2 Example temporal evolution of the instantaneous jet length $L_j(t)$. The autocorrelation-based event-selection method identifies statistically separated breakup-event minima, marked by red symbols. For this data set, the event-averaged breakup length is approximately 14 mm, whereas directly averaging all correlated frames gives approximately 18 mm. Shaded regions indicate one standard deviation about each mean.

Resolved detached droplets were analyzed from shadowgraph videos using background-difference segmentation, contour filling, nearest-neighbor tracking, and a virtual downstream gate. Each accepted droplet was counted once when its centroid crossed the gate in the flow direction. The equivalent projected diameter was calculated as $D_{\mathrm{eq}} = \sqrt{4A/\pi}\, s$, where A is the filled contour area and $s = 0.11594\,\mathrm{mm/pixel}$ is the image calibration. Quantitative droplet-size statistics were restricted to $D_{\mathrm{eq}} \geq 3s \simeq 0.35\,\mathrm{mm}$; smaller droplets and any micron-scale mist were treated as unresolved. Further details are described in Supplementary Sec. S1

3 Results and discussion

The results are organized around the physical requirements for MHz-order acoustic control of a Rayleigh-regime jet. First, we verify that the acoustic field can be guided by the liquid jet rather than being confined to the nozzle exit. We then examine how the breakup length changes with acoustic forcing amplitude and jet velocity for water. Because nozzle-base wetting can alter the effective exit condition, we next isolate its contribution before correlating the water amplitude and velocity sweeps with a reduced-order threshold correlation. We then examine fluid viscosity and the distribution of resolved gate-crossing droplets.

3.1 Acoustic transmission along the jet

A necessary condition for acoustic control is that the pressure field launched at the nozzle exit can reach the region where capillary breakup occurs. A liquid jet surrounded by air can act as an acoustic waveguide because the liquid–air interface provides a strong acoustic impedance contrast. Lonzaga et al. (2007) showed experimentally that internally excited ultrasonic radiation pressure can be guided by a free liquid jet and that the relevant cutoff frequency scales inversely with the jet diameter. For the lowest axisymmetric pressure-release mode, the cutoff frequency may be estimated as

$$f_{\mathrm{co}} = \frac{c}{2\pi}\frac{2.4048}{a}, \tag{2}$$

where c is the sound speed in the liquid and a is the local jet radius. Propagation of this mode requires the driving frequency to exceed the local cutoff frequency; below cutoff, the corresponding guided field is evanescent.

For water, using $c = 1480\,\mathrm{m/s}$ and $f = 6.7\,\mathrm{MHz}$ gives a limiting radius of $a \approx 80\,\mu\mathrm{m}$. The intact jets observed here have local radii of order 100–500 µm before breakup, so the 6.7 MHz excitation is above the estimated cutoff along the observed intact length. This supports the interpretation that acoustic radiation pressure can act as a distributed forcing along the jet, rather than only as a localized mechanical disturbance at the nozzle. The same conclusion is consistent with the visual appearance of surface corrugations over the intact portion of the acoustically actuated jet.

3.2 Effect of acoustic forcing amplitude

In the absence of ultrasound, the jet breaks up into droplets via the Rayleigh–Plateau instability. For an inviscid cylindrical jet, the most amplified varicose mode satisfies $kR \simeq 0.697$, corresponding to

$$\lambda_{\mathrm{max}} \simeq 4.51 d, \tag{3}$$

where $R = d/2$ is the jet radius (Rayleigh 1878; Eggers and Villermaux 2008). This wavelength is the dominant disturbance wavelength or droplet-spacing scale, not the breakup length itself. The measured breakup length is instead a convective growth distance over which an initial disturbance grows from an effective amplitude a_0 to a nonlinear pinch-off amplitude. In the simplest convective picture,

$$L_b \sim \frac{u_0}{s_{\mathrm{max}}} \ln\left(\frac{R}{a_0}\right), \tag{4}$$

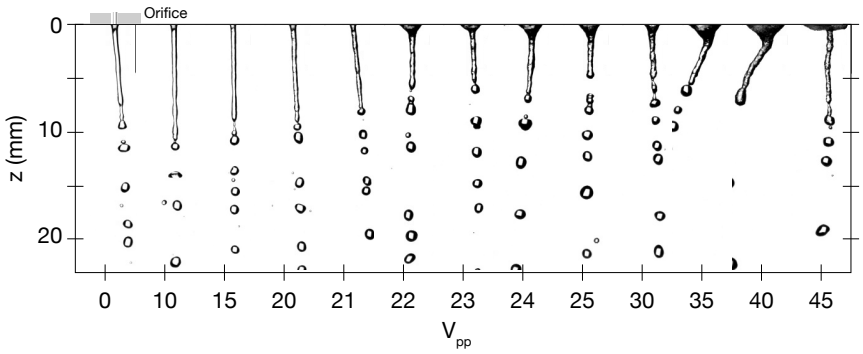


Fig. 3 Representative snapshots of the water jet at increasing input voltages with We = 5.5 and Oh = 0.0038. The horizontal axis is the input voltage measured in peak-to-peak volts and is not linearly scaled.

where u_0 is the jet velocity and $s_{\max}$ is the temporal growth rate of the dominant unstable mode (Lin and Reitz 1998; Eggers and Villermaux 2008). Thus, L_b can span several Rayleigh wavelengths and is sensitive to the initial perturbation field, nozzle geometry, wetting state, and residual mechanical vibration.

The acoustic response is reported using the normalized breakup length $L_b^* = L_b/d$ and normalized acoustic velocity $u^* = \dot{\xi}_p/u_0$, where $\dot{\xi}_p$ is the transducer particle velocity measured by laser Doppler vibrometry at resonance. Figure 3 shows that acoustic actuation qualitatively changes the breakup morphology. Without ultrasound, the jet exhibits familiar varicose growth of capillary disturbances and breaks after several jet diameters. With increasing acoustic drive, interfacial corrugations become visible on the intact jet and the first disconnection shifts upstream. The corresponding statistics in Fig. 4 show a nonmonotonic response. At small u^*, L_b^* changes weakly and can increase slightly. Once u^* exceeds a threshold range, L_b^* decreases abruptly. At still larger u^*, the reduction saturates and partially recovers.

This behavior differs from the simplest small-amplitude forced-jet picture. In classical forced capillary jets, increasing the imposed disturbance amplitude generally shortens the breakup length because the logarithmic factor in Eq. (4) decreases (Kalaaji et al. 2003). Audio-frequency experiments showed that controlled low-frequency perturbations can select the breakup wavelength and regularize droplet formation (Donnelly and Glaberson 1966; Goedde and Yuen 1970). In contrast, the present excitation frequency is MHz-order, far above the hydrodynamic droplet-formation frequency. The interface therefore does not respond as though it were being directly shaken at the breakup frequency. Instead, the response is more consistent with acoustic radiation pressure driving a lower-frequency capillary-wave envelope through a pressure–interface feedback mechanism. A similar separation of time scales was reported by Zhang et al. (2023), who showed that MHz acoustic excitation of a sessile droplet can generate visible low-frequency capillary waves only after a finite threshold is reached.

The partial recovery of L_b^* at the largest forcing amplitudes should be interpreted cautiously. Large-amplitude forced jets can exhibit breakup reversal, in which the breakup length stagnates or increases as forcing is increased further. Denner et al. (2022) attributed this reversal to nonlinear internal flow structures, including vortex rings and local flow obstruction, that can slow or reverse neck collapse. The

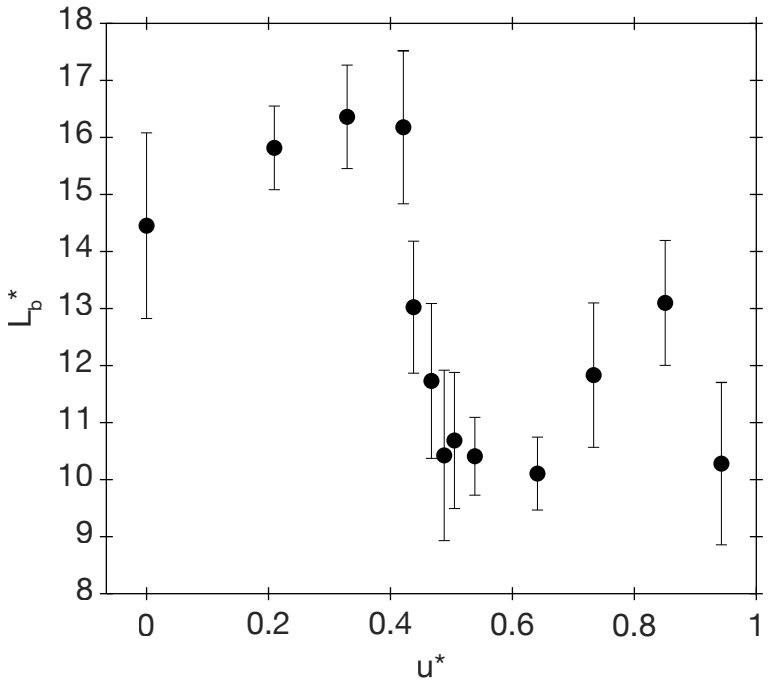


Fig. 4 Average normalized breakup length $L_b^* = L_b/d$ as a function of normalized acoustic velocity $u^* = \dot{\xi}_p/u_0$ for water at Re = 611, We = 5.5, and Oh = 0.0038. Each point represents the average of five or more physically independent recordings; error bars denote the standard deviation of retained breakup-event lengths.

present system differs because the forcing is ultrasonic and is coupled through the nozzle base rather than imposed as a prescribed inlet-velocity modulation. Nevertheless, the analogy is useful: after the acoustic field has triggered upstream capillary breakup, additional input energy may be diverted into base wetting, acoustic streaming, internal recirculation, satellite-drop formation, or competing interfacial modes rather than monotonically amplifying the same destabilizing Rayleigh mode.

3.3 Effect of jet velocity

Figures 6 and 7 show that acoustic actuation is most effective at low jet velocity. In the unforced case, L_b^* generally increases as We increases, consistent with a convective instability whose capillary growth rate does not increase as rapidly as the downstream transport speed. When the same 25 Vpp acoustic input is applied, the breakup length is substantially reduced at low We, but the difference between the forced and unforced cases decreases as the jet flow increases, reducing the residence time of the jet, and reducing the overall influence of the oscillation in the jet. At the largest flow rates, the two curves approach one another.

Two effects likely contribute to this trend. First, at fixed voltage the measured transducer velocity is approximately fixed while u_0 increases, so the normalized forcing $u^* = \dot{\xi}_p/u_0$ decreases. The acoustic forcing therefore becomes weaker relative to jet inertia. Second, the residence time over a given downstream distance decreases as u_0 increases, leaving less time for the acoustically seeded disturbance to grow before it is convected away. This is analogous to conventional forced-jet experiments, where the

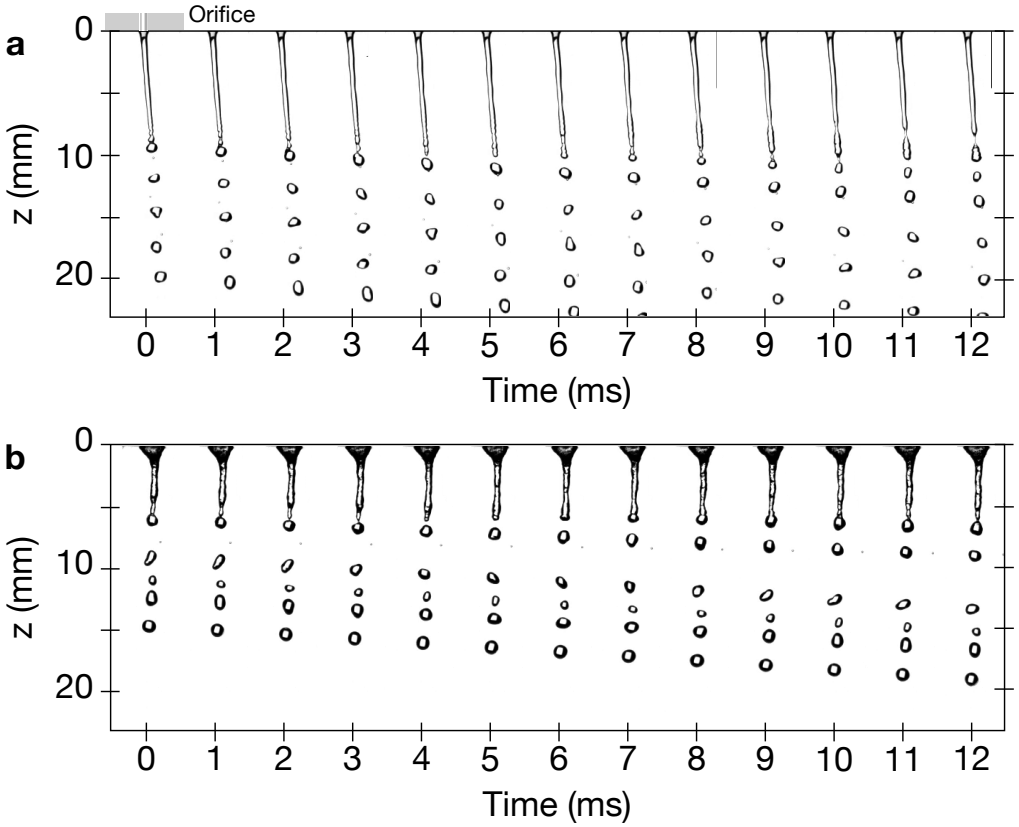


Fig. 5 Representative breakup sequences for water with (a) no ultrasound and (b) sinusoidal acoustic excitation at 25 Vpp. Conditions are Re = 611, We = 5.5, and Oh = 0.0038. Acoustic excitation shifts the first disconnection upstream and produces a more corrugated intact jet.

breakup response depends not only on disturbance amplitude but also on the matching between imposed disturbance and hydrodynamic growth process (Donnelly and Glaberson 1966; Kalaaji et al. 2003).

3.4 Effect of base wetting

In addition to direct acoustic forcing, wetting at the nozzle exit influences the measured breakup length. Apparent from Figs. 3 and 5, the fluid wets the orifice exit when applying ultrasound. This wetting widens the jet at the orifice exit to a diameter considerably larger than the orifice and the jet farther downstream. High-frequency acoustic waves propagating within a solid substrate can alter dynamic wetting and contact-line motion through the combined action of acoustic radiation pressure and boundary-layer-driven streaming. Depending on the initial surface wettability and forcing conditions, substrate vibration can promote droplet spreading or draw a thin acoustowetting film from a sessile liquid volume (Rezk et al. 2012, 2014). Because nozzle geometry and inlet disturbances are known to influence jet morphology and breakup behavior (McCarthy and Molloy 1974), this wetted region must be treated as part of the acoustic coupling pathway rather than as a purely incidental artifact. Indeed, efforts have been made in the past to avoid such wetting, as they can lead to orifice fouling and print failure in ink-jet printers (Borgelink et al. 2022; de Jong et al. 2007).

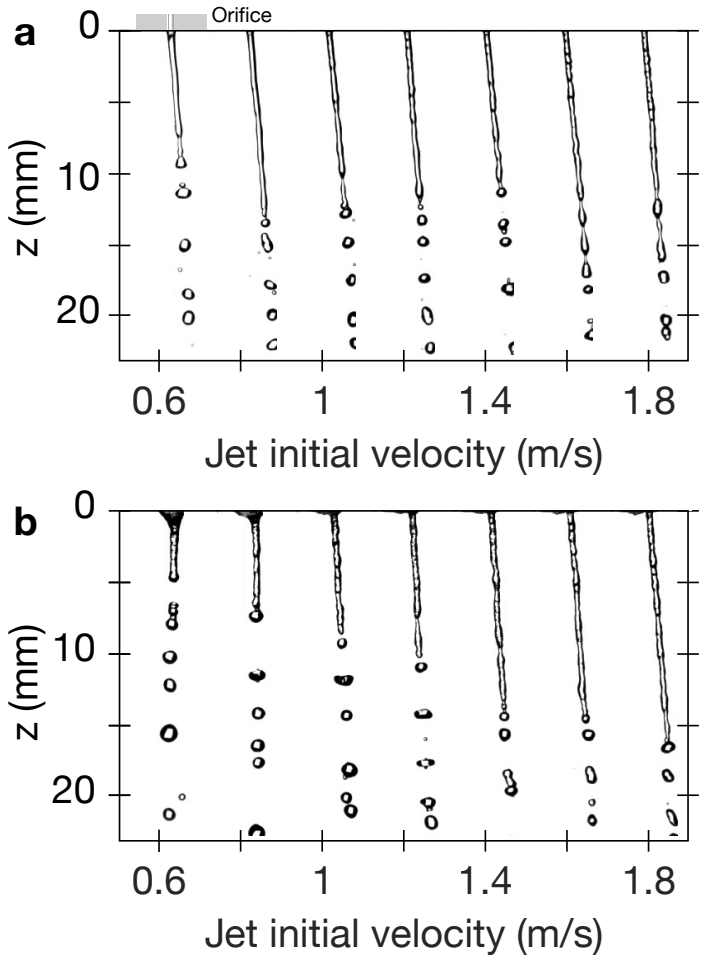


Fig. 6 Representative breakup sequences at different initial jet velocities for water with (a) no ultrasound and (b) 25 Vpp acoustic excitation. The corresponding Re and We values are listed in Supplementary Table S1.

To isolate the wetting contribution, three conditions were compared using DI water at $Q = 30\,\mathrm{mL/min}$. First, a control jet was recorded under the standard operating condition. Second, the flow rate was temporarily increased to 90 mL/min to remove the wetted base; the flow rate was then returned to 30 mL/min and the jet was recorded after confirming that no visible wetting remained at the nozzle exit. Third, a liquid droplet was intentionally placed at the nozzle exit to create a deliberately wetted base before recording.

As shown in Fig. 8, removing the wetted base increases L_b^* relative to the control, whereas intentionally introducing a wetted base substantially shortens the jet. This confirms that base wetting alone can reduce the breakup length. Mechanically, the wetted base can alter the effective exit shape, provide a larger oscillating liquid–solid contact area, and convert the transducer's thickness-mode motion into pressure disturbances normal to the liquid–air interface. The wet base therefore acts as both a geometric perturbation and an acoustic coupling element. The total breakup-length reduction observed under ultrasound should consequently be interpreted as a combined effect of guided acoustic radiation pressure, capillary-wave feedback, and wetting-mediated disturbance injection at the nozzle base. At the same time, excessive base wetting may reduce actuation efficiency because the additional liquid volume can

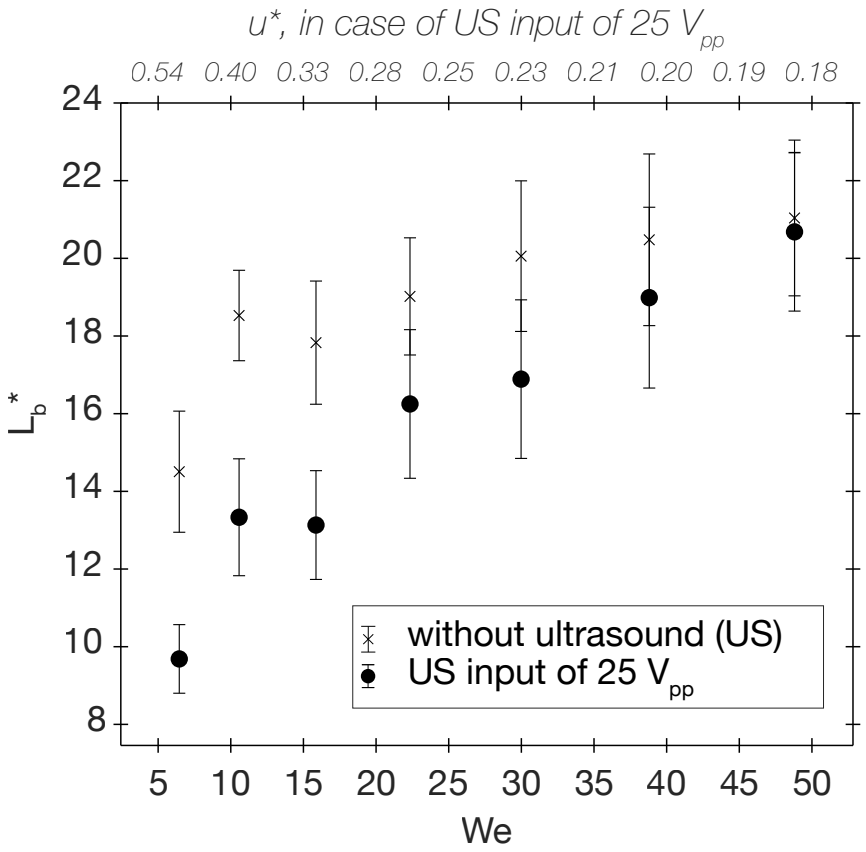


Fig. 7 Average normalized breakup length as a function of We for water with and without 25 Vpp ultrasound. The upper axis shows the corresponding $u^* = \dot{\xi}_p / u_0$ for the acoustic case and is included only for comparison.

absorb and dissipate acoustic energy while also promoting unwanted thin-film atomization on the device surface adjacent the orifice (Collins et al. 2012; Huang et al. 2019).

3.5 Reduced-order correlation of the sudden decrease in water jet breakup

The water data in Figs. 4 and 7 show two linked features: the breakup length does not decrease continuously from zero forcing, but instead decreases abruptly after a finite acoustic drive, and the shortening weakens as We approaches the upper end of the Rayleigh regime. To connect these observations, we constructed a reduced-order threshold correlation for the water jet. The correlation is not intended as a universal prediction for all tested liquids; rather, it provides a compact representation of the water-jet data and places the observed loss of acoustic efficacy near We $\simeq$ 50 on the same footing as the threshold observed in the amplitude sweep. A longer derivation is given in Supplementary Information, Sec. S2.

The underlying hydrodynamic picture is the convective growth of the Rayleigh–Plateau mode. In the absence of acoustic actuation, the measured breakup length may be written in the usual logarithmic form $L_b \sim (u_0/s_{\max}) \ln(R/a_n)$, where $R = d/2$, $s_{\max}$ is the growth rate of the dominant capillary mode, and a_n is an effective background disturbance amplitude set by the nozzle, wetting state, and residual mechanical perturbations. Acoustic actuation is represented by an additional capillary-wave amplitude that turns on only when the guided acoustic drive reaching the wetted nozzle base exceeds a threshold. The reduced

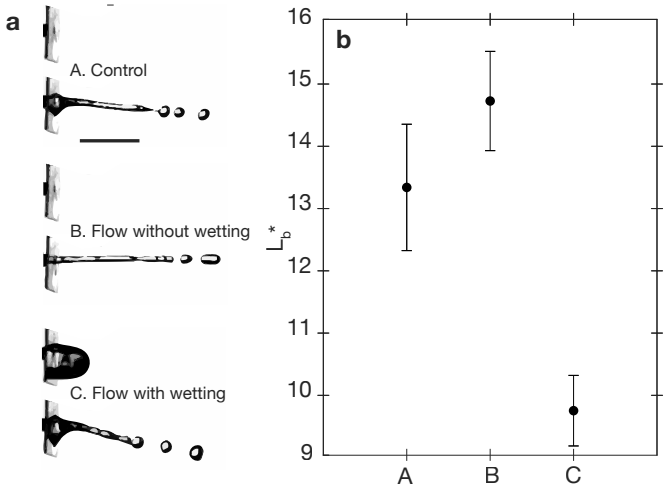


Fig. 8 Effect of base wetting on jet breakup length. (a) Representative snapshots of DI water jets under three nozzle-base conditions: A, control; B, flow without visible base wetting after high-flow conditioning; and C, flow with an intentionally introduced wetted base. (b) Normalized breakup length L_b^* for the three conditions. Removing the wetted base increases L_b^*, whereas introducing a wetted base substantially reduces L_b^*, indicating that base wetting contributes to upstream breakup. Error bars denote the standard deviation of retained breakup-event lengths.

control parameter is

$$\Theta = \left(\frac{\dot{\xi}_p}{\dot{\xi}_c}\right)^2 \frac{1}{1+\mathrm{We}/\mathrm{We}_t}, \tag{5}$$

where $\dot{\xi}_p$ is the measured transducer particle velocity, $\dot{\xi}_c$ is the critical particle velocity for onset, and We_t describes the loss of acoustic coupling as increasing inertia reduces the stable wetted base at the nozzle.

The acoustically sustained capillary-wave amplitude is represented as a saturated threshold branch,

$$\hat{A}_c = A_{\max}\left[\frac{\Theta-1}{\Theta_s+\Theta-1}\right]^{1/2} H(\Theta-1), \tag{6}$$

where $\hat{A}_c = A_c/R$, $A_{\max}$ is the normalized saturated capillary-wave amplitude, Θ_s sets the width of the post-onset transition, and H is the Heaviside distribution (Skinner and Weil 1989). Substituting this acoustically generated disturbance into the convective-growth expression gives

$$\frac{L_b}{d} = \frac{u_0}{d s_{\max}} \ln\left[\frac{R}{a_n(u_0)+R\hat{A}_c}\right]. \tag{7}$$

Here $a_n(u_0)$ is obtained from the no-ultrasound baseline for the corresponding water condition, so device-specific differences in the background nozzle state are not forced into the acoustic parameters.

A joint fit to the water amplitude sweep and water velocity sweep gives $\dot{\xi}_c = 0.29\,\mathrm{m/s}$, $\mathrm{We}_t = 126$, $A_{\max} = 0.011$, and $\Theta_s = 0.031$. The corresponding saturated acoustic capillary-wave amplitude is $RA_{\max} \approx 5.5\,\mu\mathrm{m}$. The fit gives $\chi^2/\mathrm{dof} = 1.46$, where dof refers to the number of independent data values remaining after estimating the model parameters as the "degrees of freedom" remaining, and the implied cutoff of the acoustic shortening near $\mathrm{We} \approx 50$ is consistent with the observed collapse of the water-jet actuation effect near $\mathrm{We} \approx 49$. Thus, the correlation captures the water experiments: it represents the threshold-like

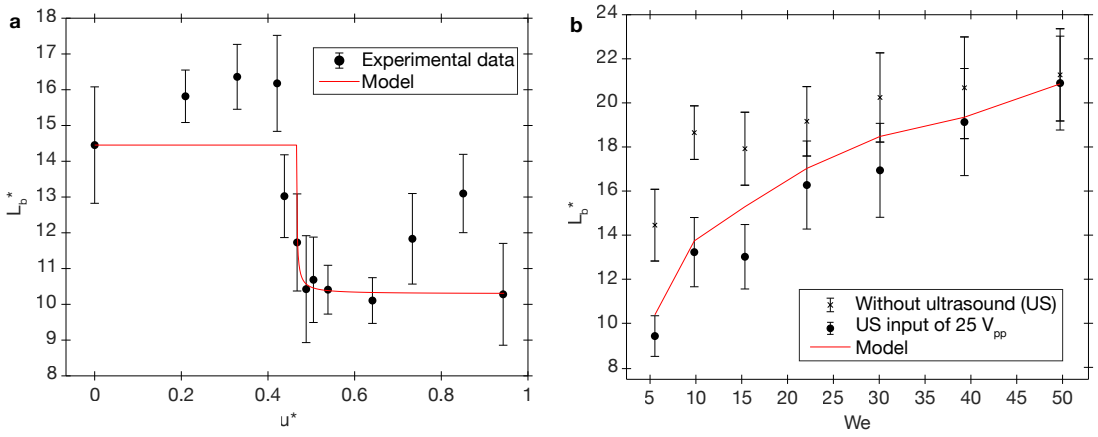


Fig. 9 Reduced-order threshold correlation for water only. (a) Normalized breakup length as a function of the normalized acoustic velocity $u^* = \dot{\xi}_p / u_0$ for the water amplitude sweep. (b) Normalized breakup length as a function of We for the water velocity sweep with and without 25 Vpp acoustic excitation. The correlation captures the water data, including the sudden reduction in breakup length and the loss of actuation efficacy near We ≃ 50.

decrease in L_b/d, the post-threshold saturation, and the weakening of the effect at high Weber number. Because the correlation was fit to both water sweeps rather than to a single low-Weber-number datum and then tested independently, we do not claim predictive validation.

This reduced-order correlation does not extend to the glycerol–water solutions. In the higher-viscosity, higher-Ohnesorge-number fluids, the jet length decreases immediately at low acoustic forcing, without the weak-response plateau and sudden onset observed in water. This immediate response indicates a different acoustic-coupling and breakup regime, likely involving stronger viscous coupling near the wetted base and a different conversion of MHz forcing into the low-frequency interfacial envelope. For this reason, the glycerol–water data are discussed phenomenologically below and are not compared to the threshold breakup uniquely seen with water.

3.6 Effect of fluid viscosity

The viscosity sweep in Figs. 10 and 11 separates capillary forcing from viscous damping, with weaker effects on surface tension and acoustic impedance through the addition of glycerol. Without ultrasound, increasing Oh lengthens the breakup length. This agrees with viscous extensions of Rayleigh's theory: viscosity dissipates interfacial motion, reduces the temporal growth rate of unstable capillary modes, and therefore increases the convective distance required for a disturbance to reach pinch-off amplitude (Weber 1931; Eggers and Villermaux 2008). Acoustic excitation reduces L_b^* for all four fluids, but the shape of the response changes with Oh.

Water shows a relatively sharp transition from a weak-response branch to a shortened-jet branch. The glycerol–water mixtures exhibit an immediate decrease in L_b^* at low forcing and then remain reduced over a broader range of forcing amplitudes. This contrast indicates that the higher-viscosity, higher-Oh fluids do not share the same thresholded water response. Viscosity likely plays two opposing roles. On one hand, viscosity damps capillary growth and lengthens the unforced jet. On the other hand, the longer

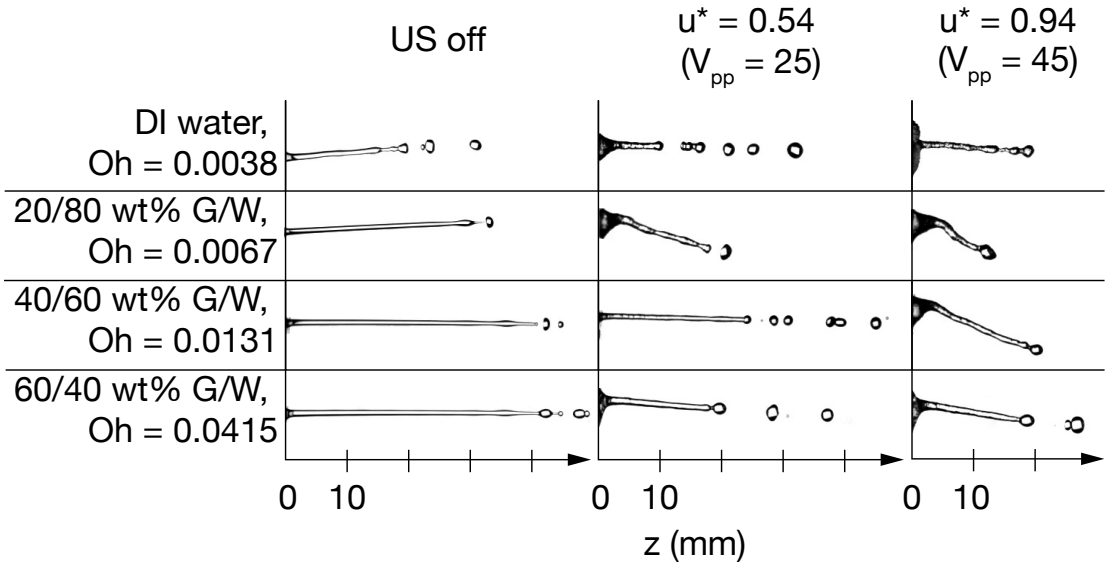


Fig. 10 Representative snapshots of jet breakup for fluids with different viscosities under acoustic excitation. Rows correspond to DI water, 20/80 wt% glycerol–water, 40/60 wt% glycerol–water, and 60/40 wt% glycerol–water, with Oh = 0.0038, 0.0067, 0.0131, and 0.0415, respectively. Columns compare the unforced case, acoustic excitation at 25 Vpp with $u^* = 0.54$, and acoustic excitation at 45 Vpp with $u^* = 0.94$.

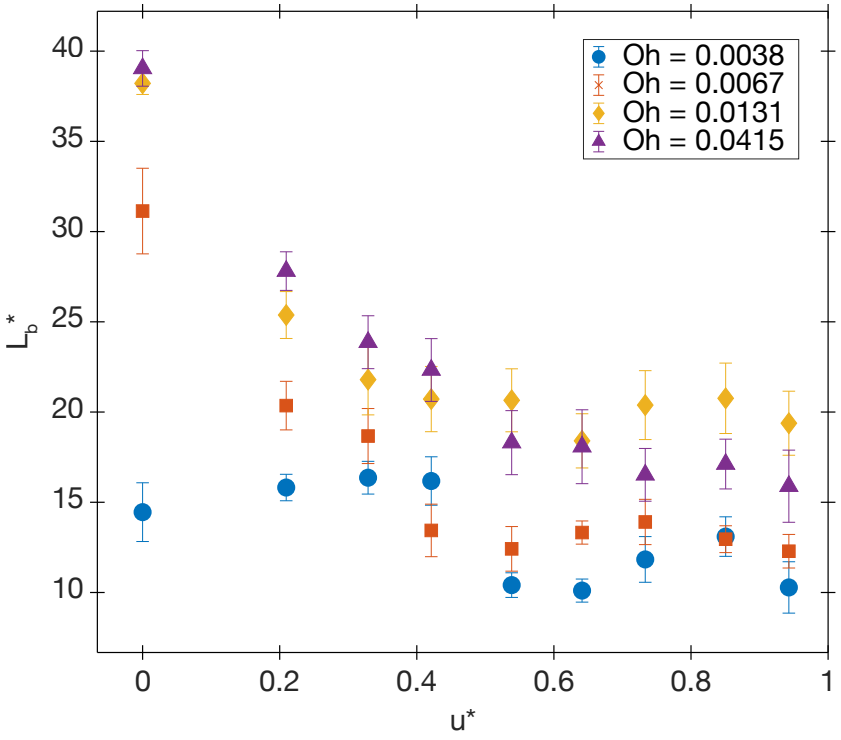


Fig. 11 Average normalized breakup length for four fluids as a function of normalized acoustic velocity at approximately fixed Weber number, We ≈ 5.5–6.8. Increasing Oh lengthens the unforced jet, while acoustic excitation reduces L_b^* across all tested fluids. The higher-viscosity glycerol–water solutions respond immediately to forcing and are not compared to the water-threshold correlation.

unforced growth distance provides a larger window over which acoustic disturbances can accumulate, and viscous coupling near the wetted base can convert substrate vibration into a lower-frequency interfacial response more directly. Similar sensitivity to Oh is observed in large-amplitude forced-jet studies, where viscous stresses and finite-amplitude internal flow structures control whether breakup reversal and mode competition appear (Denner et al. 2022).

The present data therefore support a combined mechanism. Acoustic radiation pressure increases the effective initial disturbance amplitude and modifies the pressure distribution near the intact jet, while viscosity controls how this disturbance is dissipated, phase shifted, and converted into hydrodynamic capillary motion. Within the tested range, increased viscosity does not eliminate acoustic control. Instead, it changes the response from the threshold-like behavior observed in water to an immediate shortening regime. At still larger Oh, however, one would expect overdamping to eventually suppress the acoustic effect as the capillary mode itself becomes too strongly damped to grow efficiently.

3.7 Resolved gate-crossing droplet-size distributions

We next examine the detached visible droplet population. Figure 12 reports the normalized equivalent diameter $D^*_{\mathrm{eq}} = D_{\mathrm{eq}}/d$ of resolved gate-crossing droplets of size greater than a noise-reducing three-pixel cutoff. For classical Rayleigh breakup of a cylindrical jet, volume conservation applied to the dominant Rayleigh wavelength gives a primary droplet diameter of approximately $D_R \simeq 1.89d$ (Rayleigh 1878; Eggers and Villermaux 2008); the resolved gate-crossing droplets in Fig. 12 lie mainly between $1.5d$ and slightly above $2d$, consistent with this classical breakup scale despite the use of MHz ultrasound excitation. The data should be interpreted as distributions of optically resolved millimeter-scale objects sampled by the virtual gate, not as complete spray distributions. This distinction is important because classical ultrasonic atomization and modern ultrasonic-nebulizer studies show that MHz capillary-wave atomization can generate much smaller droplets than what can be resolved at the present magnification (Lang 1962; Kooij et al. 2019). Thus, any sub-resolution mist produced near the vibrating nozzle or droplet field is outside the quantitative size range of Fig. 12.

In the fixed-flow voltage sweep at We = 5.56 and Oh = 0.0038 (Fig. 12a), the resolved droplet distribution changes only modestly at low and intermediate u^*, but high forcing produces distribution-level shifts relative to the unforced case. The largest shifts occur at $u^* = 0.54$, 0.64, and 0.94, which are also in the actuation range where the breakup-length data show strong acoustic modification. The median visible droplet diameter does not decrease monotonically with acoustic forcing. Instead, the high-u^* cases contain a visibly larger upper portion of the resolved distribution.

The flow-rate sweep provides the complementary comparison at fixed acoustic drive (Fig. 12b). At each Weber number, the 25 V_{pp} case is compared with the corresponding unforced case using the same region of interest (ROI) and gate for that flow rate. Acoustic actuation shifts the resolved diameter distribution upward for most of the Rayleigh-regime conditions, with differences from We ≈ 6 through We ≈ 39. At We ≈ 50, where the breakup-length reduction also weakens as the jet flow speed increases, reducing the relative amplitude of the acoustic forcing over the intrinsic velocity of the jet, causing the on/off difference in the resolved diameter distribution to be less pronounced. The droplet-size data therefore reinforce the

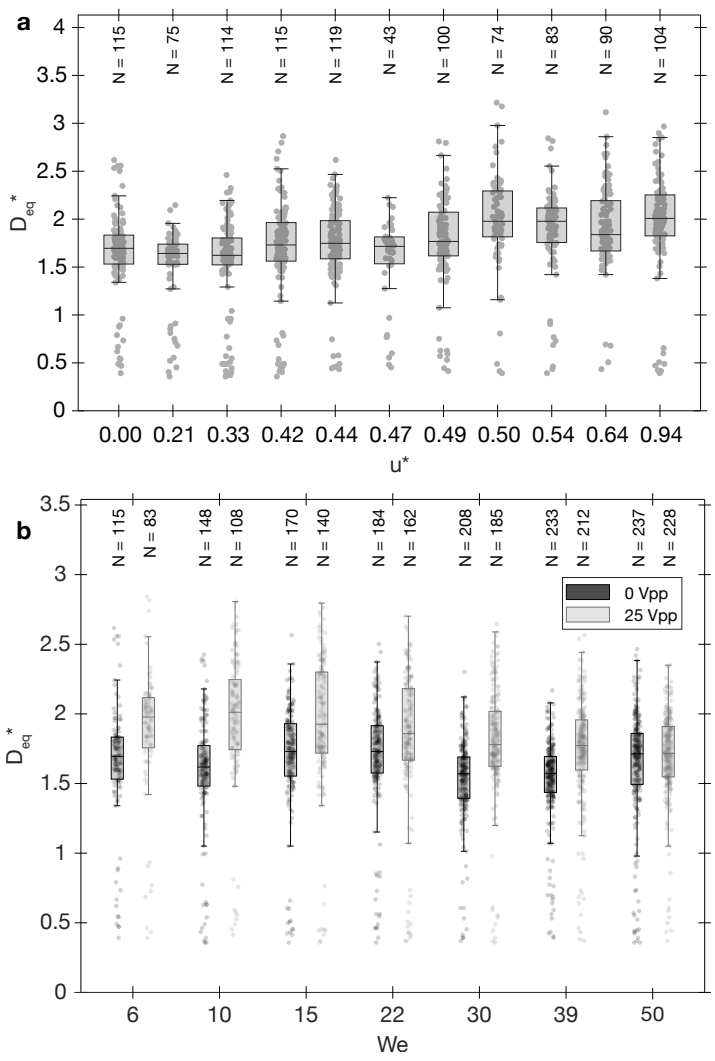


Fig. 12 Resolved gate-crossing droplet-size distributions. (a) Normalized equivalent droplet diameter $D^*_{\mathrm{eq}} = D_{\mathrm{eq}}/d$ as a function of normalized acoustic velocity $u^* = \dot{\xi}_p/u_0$ for DI water at $Q = 30\,\mathrm{mL/min}$, We = 5.56, and Oh = 0.0038. (b) D^*_{eq} as a function of Weber number for DI water with no ultrasound and with 25 V_{pp} acoustic excitation. Each box shows the median and interquartile range of resolved gate-crossing droplets after the three-pixel cutoff; points are individual retained gate-crossing droplets, and N gives the number of retained droplets in each condition. Since repeat videos of the experiments were not available, significance of differences are not discussed.

same physical picture obtained from L^*_b: MHz excitation strongly modifies the breakup process at low and moderate We, but its relative influence weakens as jet inertia increases.

4 Conclusions

We have shown that MHz-order acoustic excitation applied directly at the nozzle exit can substantially modify Rayleigh-regime liquid jet breakup in quiescent air. A through-hole thickness-mode lithium niobate transducer operating near 6.7 MHz generated visible interfacial corrugations and shifted the breakup point upstream. By analyzing high-speed shadowgraphy data with an autocorrelation-based event-selection method, we separated instantaneous jet-length fluctuations from statistically independent breakup events and quantified the normalized breakup length L_b/d.

The acoustic response depends on forcing amplitude, jet velocity, viscosity, and base wetting. For water at low Weber number, increasing acoustic forcing produced a threshold-like reduction in L_b/d, followed by saturation and partial recovery at large We. A reduced-order threshold correlation was fit to the water amplitude and velocity sweeps and captured the sudden decrease in L_b/d and the loss of acoustic efficacy near We $\simeq 50$. Because the correlation was not validated against independent conditions, it should be interpreted as a compact representation of the water data rather than as a predictive theory. At fixed acoustic voltage, the reduction weakened as We increased because the normalized forcing $u^* = \dot{\xi}_p/u_0$ decreased, the disturbance had less residence time to grow, and the wetted-base coupling path weakened near the wind-influenced transition.

The glycerol–water mixtures did not follow the water-threshold behavior. Instead, the higher-viscosity, higher-Ohnesorge-number fluids shortened immediately at low forcing, indicating a different acoustic-coupling and breakup regime. Increasing viscosity lengthened the unforced jet but did not suppress acoustic control over the tested range. Base-wetting experiments showed that a wetted nozzle base independently reduces L_b/d, confirming that wetting-mediated coupling is an important part of the mechanism.

Resolved droplet tracking showed that the acoustic field also changes the visible detached droplet population. For water, high normalized forcing and fixed-voltage excitation across most of the Rayleigh-regime flow sweep shifted the distributions of gate-crossing D^*_{eq} relative to the corresponding controls. These data do not show a simple monotonic reduction in resolved droplet diameter; rather, they indicate that MHz excitation changes the breakup pathway and the distribution of visible millimeter-scale fragments. Droplets below the three-pixel optical cutoff and any micron to submicron-scale atomized mist remain unresolved in the present measurements.

Future work should quantify the full spray-size distribution using higher-magnification imaging, laser diffraction, or phase-Doppler diagnostics, measure internal flow or streaming near the nozzle base, and independently vary We, Oh, and u^* to separate inertia, viscous damping, and acoustic coupling effects. These results establish MHz-order acoustics as a compact and tunable approach for controlling free-surface jet breakup without requiring electrical, magnetic, or chemical modification of the fluid.

Authors' contributions

K.N., K.A., and J.F. conceived the study. K.N. designed and fabricated the nozzle–transducer assembly, performed the experiments, analyzed the high-speed-imaging data, and prepared the initial manuscript draft. J.F. supervised the project, developed the reduced-order data correlation, and contributed to interpretation of the acoustic and fluid-mechanics results. K.N., K.A., and J.F. revised the manuscript. All authors reviewed and approved the final manuscript.

Acknowledgments

Fabrication was performed in part at the San Diego Nanotechnology Infrastructure (SDNI) of UCSD, a member of the National Nanotechnology Coordinated Infrastructure, which is supported by the National Science Foundation (Grant ECCS–1542148). The authors wish to express their gratitude to Professor Nigel Goldenfeld (UCSD) and Professor Philip Marston (Univ. Washington) for discussions regarding this work.

Funding

The authors declare that financial support was received for the research, authorship, and/or publication of this article. This work was supported by funding from the Office of Naval Research, United States, under grant No. 13423461 to J.F. and K.A. Additional support for K.N. was provided by the STARS Fellowship.

Data availability

All data associated with this manuscript is available online at https://doi.org/10.6075/J02N52F5.

Competing interests

The authors declare that they have no competing interests.

References

Borgelink, B.T.H., Berenschot, E.J.W., Sanders, R.G.P., Schlautmann, S., Tas, N.R., Gardeniers, H.J.G.E.: Fabrication and characterization of microfluidic pedestal nozzles enabling geometric contact line pinning. Sensors and Actuators B: Chemical **365**, 131943 (2022) https://doi.org/10.1016/j.snb.2022.131943

Bertin, N., Wunenburger, R., Brasselet, E., Delville, J.-P.: Liquid-column sustainment driven by acoustic wave guiding. Physical Review Letters **105**(16), 164501 (2010) https://doi.org/10.1103/PhysRevLett.105.164501

Collins, R.T., Harris, M.T., Basaran, O.A.: Breakup of electrified jets. Journal of Fluid Mechanics **588**, 75–129 (2007) https://doi.org/10.1017/S0022112007007409

Collins, D.J., Manor, O., Winkler, A., Schmidt, H., Friend, J.R., Yeo, L.Y.: Atomization off thin water films generated by high-frequency substrate wave vibrations. Physical Review E **86**(5), 056312 (2012) https://doi.org/10.1103/PhysRevE.86.056312

Denner, F., Evrard, F., Castrejón-Pita, A.A., Castrejón-Pita, J.R., Wachem, B.: Reversal and inversion of capillary jet breakup at large excitation amplitudes. Flow, Turbulence and Combustion **108**(3), 843–863

(2022) https://doi.org/10.1007/s10494-021-00291-w

Donnelly, R.J., Glaberson, W.: Experiments on the capillary instability of a liquid jet. Proceedings of the Royal Society of London. Series A. Mathematical and Physical Sciences **290**(1423), 547–556 (1966) https://doi.org/10.1098/rspa.1966.0069

Eggers, J., Villermaux, E.: Physics of liquid jets. Reports on Progress in Physics **71**(3), 036601 (2008) https://doi.org/10.1088/0034-4885/71/3/036601

Frommhold, P.E., Lippert, A., Holsteyns, F.L., Mettin, R.: High-speed monodisperse droplet generation by ultrasonically controlled micro-jet breakup. Experiments in Fluids **55**(4), 1716 (2014)

Goedde, E.F., Yuen, M.C.: Experiments on liquid jet instability. Journal of Fluid Mechanics **40**(3), 495–511 (1970) https://doi.org/10.1017/S0022112070000289

Huang, Q.-Y., Hu, H., Han, J.-L., Lei, Y.-L., Yang, X.-Q.: Influence of waterproof films on the atomization behavior of surface acoustic waves. Micromachines **10**(11), 794 (2019) https://doi.org/10.3390/mi10110794

de Jong, J., Reinten, H., Wijshoff, H., Berg, M., Delescen, K., Dongen, R., Mugele, F., Versluis, M., Lohse, D.: Marangoni flow on an inkjet nozzle plate. Applied Physics Letters **91**(20), 204102 (2007) https://doi.org/10.1063/1.2812473

Kooij, S., Astefanei, A., Corthals, G.L., Bonn, D.: Size distributions of droplets produced by ultrasonic nebulizers. Scientific Reports **9**, 6128 (2019) https://doi.org/10.1038/s41598-019-42599-8

Kalaaji, A., Lopez, B., Attané, P., Soucemarianadin, A.: Breakup length of forced liquid jets. Physics of Fluids **15**(9), 2469–2479 (2003) https://doi.org/10.1063/1.1593023

Lang, R.J.: Ultrasonic atomization of liquids. The Journal of the Acoustical Society of America **34**(1), 6–8 (1962) https://doi.org/10.1121/1.1909020

Lin, S.P.: Breakup of Liquid Sheets and Jets. Cambridge University Press, Cambridge (2003). https://doi.org/10.1017/CBO9780511547096

Lad, V.N., Murthy, Z.V.P.: Breakup of free liquid jets influenced by external mechanical vibrations. Fluid Dynamics Research **49**(1), 015503 (2016) https://doi.org/10.1088/0169-5983/49/1/015503

Lefebvre, A.H., McDonell, V.G.: Atomization and Sprays, 2nd edn. CRC Press, Boca Raton (2017). https://doi.org/10.1201/9781315120911

Lonzaga, J.B., Osterhoudt, C.F., Thiessen, D.B., Marston, P.L.: Liquid jet response to internal modulated ultrasonic radiation pressure and stimulated drop production. The Journal of the Acoustical Society of America **121**(6), 3323–3330 (2007) https://doi.org/10.1121/1.2734493

Lin, S.P., Reitz, R.D.: Drop and spray formation from a liquid jet. Annual Review of Fluid Mechanics **30**, 85–105 (1998) https://doi.org/10.1146/annurev.fluid.30.1.85

Marr-Lyon, M.J., Thiessen, D.B., Marston, P.L.: Stabilization of a cylindrical capillary bridge far beyond the Rayleigh–Plateau limit using acoustic radiation pressure and active feedback. Journal of Fluid Mechanics **351**, 345–357 (1997) https://doi.org/10.1017/S002211209700726X

Marr-Lyon, M.J., Thiessen, D.B., Marston, P.L.: Passive stabilization of capillary bridges in air with acoustic radiation pressure. Physical Review Letters **86**(11), 2293–2296 (2001) https://doi.org/10.1103/PhysRevLett.86.2293

McCarthy, M.J., Molloy, N.A.: Review of stability of liquid jets and the influence of nozzle design. The Chemical Engineering Journal **7**(1), 1–20 (1974) https://doi.org/10.1016/0300-9467(74)80021-3

Rayleigh, L.: On the instability of jets. Proceedings of the London Mathematical Society **s1-10**(1), 4–13 (1878) https://doi.org/10.1112/plms/s1-10.1.4

Rezk, A., Manor, O., Friend, J.R., Yeo, L.Y.: Unique fingering instabilities and soliton-like wave propagation in thin acoustowetting films. Nature Communications **3**(1167) (2012)

Rezk, A., Manor, O., Yeo, L.Y., Friend, J.R.: Double flow reversal in thin liquid films driven by MHz order surface vibration. Proceedings of the Royal Society A **470**(20130765) (2014)

Shimasaki, S., Taniguchi, S.: Formation of uniformly sized metal droplets from a capillary jet by electromagnetic force. Applied Mathematical Modelling **35**(4), 1571–1580 (2011) https://doi.org/10.1016/j.apm.2010.09.033

Skinner, R., Weil, J.A.: An introduction to generalized functions and their application to static electromagnetic point dipoles, including hyperfine interactions. American Journal of Physics **57**(9), 777–791 (1989) https://doi.org/10.1119/1.15893

Weber, C.: Zum zerfall eines flüssigkeitsstrahles. ZAMM – Journal of Applied Mathematics and Mechanics **11**(2), 136–154 (1931) https://doi.org/10.1002/zamm.19310110207

Yang, C., Qiao, R., Mu, K., Zhu, Z., Xu, R.X., Si, T.: Manipulation of jet breakup length and droplet size in axisymmetric flow focusing upon actuation. Physics of Fluids **31**(9), 091702 (2019) https://doi.org/10.

1063/1.5122761

Zhang, S., Orosco, J., Friend, J.: Onset of visible capillary waves from high-frequency acoustic excitation. Langmuir **39**(10), 3699–3709 (2023) https://doi.org/10.1021/acs.langmuir.2c03403

Supplementary Files

This is a list of supplementary files associated with this preprint. Click to download.

- supplementary.pdf